Indian Journal of Pure & Applied Physics
Vol. 59, May 2021, pp. 398-403

Improved Photocatalytic Properties of Bismuth Molybdate Prepared by using High Energy Ball Milling Technique for Degradation of Rhodamine B

Shomaila Khanam, Mangaraj Pradhan & Sanjeeb Kumar Rout
Department of Physics, Birla Institute of Technology, Mesra, Ranchi, Jharkhand-835 215

Received 8 January 2021; accepted 12 February 2021

Bismuth molybdate (Bi_2MoO_6) was prepared through the solid-state route in the stoichiometric ratio followed by ball milling. The high-energy ball milling reduced the crystalline size from 96 to 35nm and increased the surface area from 0.351616 to10.7256 m^2/g in 5h. No structural change was observed. The comparative study of the photo catalytic activity for the decolorization of Rhodamine B (RhB) in the presence of UV light has been done by employing 5h milled Bi_2MoO_6 and unmilled Bi_2MoO_6 as a catalyst has been done. The dye degradation was observed by a decrease in the absorption spectrum and decolorization in the presence of UV irradiation. The 5h milled Bi_2MoO_6 proved to be the efficient photocatalyst over unmilled Bi_2MoO_6. The degradation efficiency of the unmilled and 5h ball milled (Bi_2MoO_6) catalyst, observed in RhB was found to be 30 and 80% respectively. The degradation efficiency was found to be dependent on the size of the catalyst added in the dye solution may be due to increased surface area provided the increased number of active sites for the reaction. Therefore, 5h ball-milled Bi_2MoO_6 can act as a catalyst for the treatment of noxious and imperishable organic pollutants in water.

Keywords: Photocatalysis, Electron scavengers, Photo-degradation, Rhodamine B

1 Introduction

The increment in water pollution has led to extensive research of photocatalytic systems. Honda and Fujishima were the first to report the photocatalysis of water with TiO_2 under light irradiation[1]. Since then, numerous researches have been done where different synthesis techniques and different materials of the photocatalyst have been employed. Photocatalysis is a modern technique for the degradation of dyes. The process is similar to the Advanced Oxidation process (AOP) and involves the production of electron-hole pairs on illumination with an appropriate wavelength of light.

Semiconductor photocatalysis has proven to be a promising alternative to conventional AOPs. It has received massive attention for water treatment due to its efficiency in degrading toxic elements of water and converting them into nonharmful compounds without expensive chemical usage [2-5]. Till now, various semiconductors TiO_2 [6], WO_3 [7], Mn_2O_3 [8], V_2O_5 [9], ZnO[10], CdO [11], and CuO[12] has been studied for photocatalytic dye-water treatment. The interesting properties of metal tungstate such as dielectric capacity, ion conductive, luminescent, and catalytic properties have verified it as promising candidates for this purpose. W.Zhang *et al* [13,14] reported that both the size and the morphology affect the intrinsic features of semiconductor oxides. Smaller size photocatalysts are accepted to perform better than larger size due to higher separation efficiency of electron-hole pair and higher surface-to-volume ratio. Photocatalysis has proved to be significant in solving water contamination problems.

In this study, the morphological and structural properties of 5h milled and unmilled Bi_2MoO_6 photocatalyst were examined. The photocatalytic activity of the prepared structures was monitored for the degradation of RhB under UV irradiation. The effect of parameters like size, surface area, and reusability is explored. Several methods such as solid-state reaction[15], sol-gel [16], hydrothermal[17,18], precipitation[19,20], and sonochemical[21] have been served to prepare bismuth tung state photocatalysts. Among them, the SSR route has proved to be cost-effective and eco-friendly. The SSR technique produces the catalyst in bulk proportion so that it could efficiently be employed in industries.

2 Materials and Methods

2.1 Synthesis of Bi_2MoO_6

The synthesis of Bi_2MoO_6 ceramic was done by a cost-effective solid-state reaction technique. The stoichiometrically calculated Bi_2O_3 and MoO_3 were thoroughly ground in the liquid medium for 6h. The

*Corresponding author (E-mail:skrout@bitmesra.ac.in)

ceramic powder mixture then, calcined at 500 °C for 24h with an intermediate grinding. The monophasic Bi_2MoO_6 ceramic was pulverized for 5h in an aqueous phase in a planetary ball mill. The ball to powder ratio was maintained at 10:1. The planetary ball mill speed was set at 200 rpm. The ball-milled sample was dried and grounded. Phase stability before and after ball milling was observed by an FTIR and XRD spectrometer.

2.2. Characterization

XRD analysis was performed on a diffractometer (Rigaku-DMax, Japan) with Cu-Kα radiation (λ = 0.15418 nm). Fourier transform infrared (FTIR) spectra were examined using IR-prestige 21, Shimadzu, FTIR spectrometer using KBr as a diluting agent in the frequency range 400 to 4,000cm^{-1}. Raman spectrum was recorded by using a Raman spectrophotometer (Renishaw, in Via, UK). A study of pore size distribution and surface area was performed using a BET (Nova touch-LX1, Quantachrome) apparatus. UV–vis absorbance spectra were observed using a UV–vis spectrophotometer (Lambda 35, Perkin Elmer, Singapore) within the wavelength ranging from 200 to 800 nm. Photoluminescence (PL) spectra were analyzed using a fluoro spectrophotometer (Lambda 35, Perkin Elmer, Singapore).

2.3. Photodegradation of RhB

The photocatalytic test was performed under UV irradiation in a photoreactor chamber. The degradation of RhB dye was monitored from the absorbance spectra, which were examined by a UV-vis spectrometer (Lambda 35, Perkin-Elmer, USA). 20 mg of Bi_2MoO_6 catalyst was added in a pyrex glass beaker containing 100ml of dye solution. The dye solution with the catalyst was continuously stirred for 1h at 300 rpm without light irradiation so that the dye molecule gets adsorbed on the surface of the prepared Bi_2MoO_6. The dye-catalyst mixture was placed in the photocatalytic chamber installed with UV bulbs of power 72 watts. The dye-catalyst mixture was set at a distance of 13cm from and UV lamp. After every one-hour interval, 3 to 4 ml of aliquots were separated from the catalyst in a centrifuge (Remi PR-24) and observed under UV-vis spectrometer. The degradation efficiency was calculated from the formula

$$\eta = \left(\frac{A_0 - A_t}{A_0}\right) \times 100$$

And the reaction rate constant was calculated from the formula $\ln\left({}^{A_0}/_{A_t}\right) = -K_{app}\, t$

Where, K_{app} is the apparent first-order rate constant.

3. Results and discussion

3.1. Structural analysis

Figure 1 represents the x-ray diffractogram of unmilled and 5h milled bismuth molybdate. The x-ray diffraction pattern depicts the orthorhombic symmetry of the prepared photocatalyst which is completely following the JCPDS card no 76-2388[22, 23]. The diffractogram shows the monophasic nature of Bi_2MoO_6 which was maintained after ball milling as well. But a noticeable change in the diffraction peaks was observed. The diffraction peaks became gradually broader, thus representing that the average crystallite size decreases with ball milling. The surface area analysis through the BET technique using N_2 adsorption-desorption shows that the surface area of unmilled Bi_2MoO_6 at 800 °C was 0.351616 m²/g and that of milled powder the surface area rose to 10.7256 m²/g. There is a ten times increase in 5h milled Bi_2MoO_6.

Figure 2(a) shows the FTIR spectra of milled and unmilled Bi_2MoO_6 in the frequency ranging from 4000 to 400 cm^{-1}. The absorption peak at 3390cm^{-1} and 1647cm^{-1} represents O-H bending and stretching vibration modes[24]. The characteristic peak at 1573 cm^{-1} shows a strong C=C bond [25]. The absorption peak at 1215 cm^{-1} shows the C-O stretching mode due to the absorption of CO2 on the Bi_2MoO_6 surface. The absorption peaks at 827 and 703 cm^{-1} show Mo-O bond and the 543 cm^{-1} absorption peak shows Bi-O bond[26-29]. No change in band positions was observed for 5h ball milled Bi_2MoO_6 powder, suggesting that there is no change in crystal symmetry.

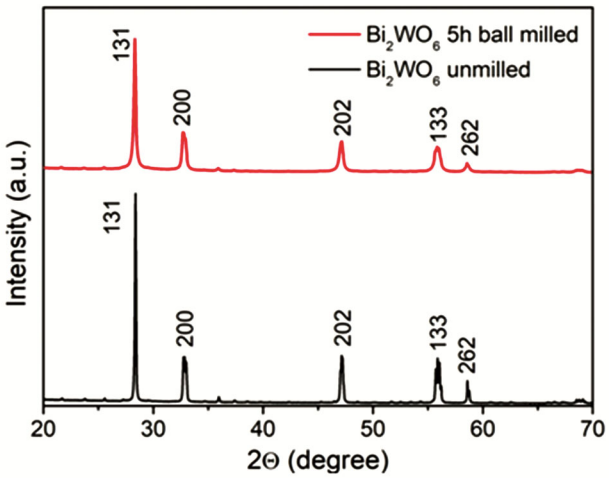

Fig. 1 — XRD diffractograph of Bi_2MoO_6 unmilled and 5h ball-milled.

Figure 2(b) shows the Raman spectra of unmilled and 5h ball-milled Bi_2MoO_6 at room temperature. Both the spectra show an indistinguishable pattern, suggesting no structural change occurred with the decrease in the size of Bi_2MoO_6 due to ball milling. All the peaks of Bi_2MoO_6 were recognized in the range from 200 to 1000 cm^{-1}. The characteristic band at 285 cm^{-1} shows the bending vibration mode of MoO_6 octahedra[30], and the others at 329, 357 & 407 cm^{-1} show the symmetry mode bending vibration of MoO_6 octahedra. The spectrum 791cm^{-1} shows a very strong band which represents the MoO_6 octahedron symmetric stretch[31]. The mid-intensity band 715 & 850 cm^{-1} appear in an Alg nature due to the orthorhombic twist of the octahedron[32-34].

3.2 Optical properties.

Figure 3a presents the optical band gap of unmilled and 5h milled Bi_2MoO_6, calculated by the Kubelka-Munk equation. The Kubelka-Munk function is given by the formula $[F(R)\ h\nu]^{1/n} = C_1\ (E_{gap} - h\nu)$[35-37]. The optical energy band gap of the Bi_2MoO_6 unmilled and Bi_2MoO_6 5h ball-milled was calculated to be 3.49 and 2.59 eV, determined by tauc plot as shown in Fig. 3a.

Figure 3 (inset) shows PL spectra of Bi_2MoO_6 unmilled and 5h ball-milled powders. The strong PL intensity of unmilled Bi_2MoO_6 represents a higher recombination rate of photogenerated electron-hole pairs[38] and the weaker PL intensity of 5h milled Bi_2MoO_6 represents a lower recombination rate. Thus PL result is following the photocatalytic result discussed subsequently.

3.3 Degradation of RhB

It is reported that RhB has maximum absorption at 554 nm. Fig. 4(a) and 4(b) show the photocatalytic activity of unmilled and 5h ball-milled Bi_2MoO_6 photocatalyst, whose performance was observed by the degradation of RhB under ultraviolet irradiation. 5h milled Bi_2MoO_6 proves to excel in RhB degradation than unmilled Bi_2MoO_6. The degradation rate of 85% is achieved by 5h milled Bi_2MoO_6 whereas only 30% of RhB was degraded by unmilled Bi_2MoO_6 in 9h. The ball milling played an important part in improving the degradation efficiency of the photocatalyst. It reduced the size of the prepared photocatalyst which might have increased the adsorption and the active site of the reaction. After every hour the absorbance spectra showed a dropped down, indicating the reduction in the concentration of RhB. As the irradiation time increased hypsochromic shift was observed in the UV spectra of RhB dye. This is due to the N-de-ethylation of RhB, which has

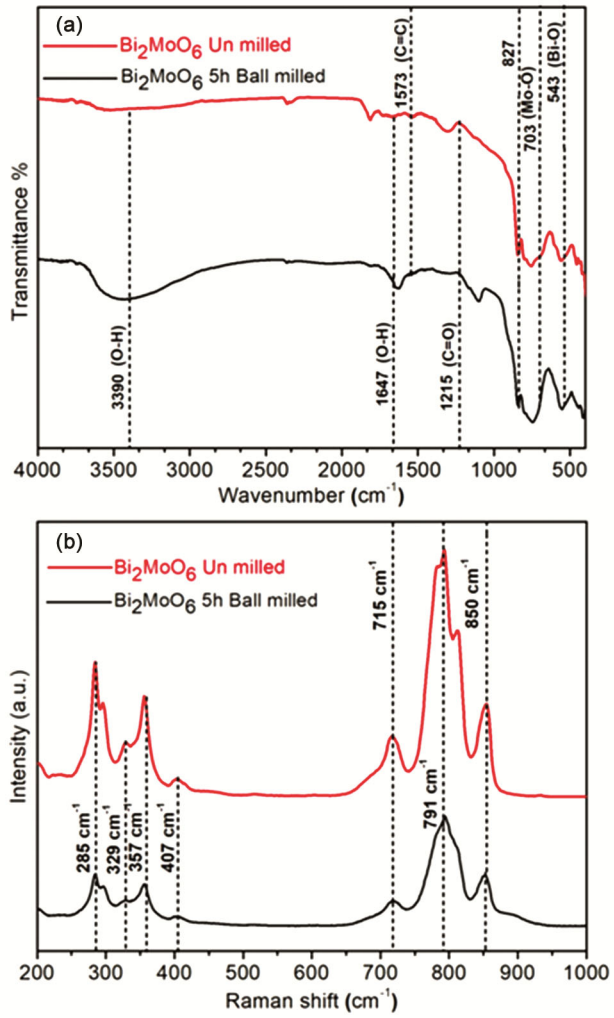

Fig. 2 — (a) & (b) shows the FTIR and Raman spectra of Bi_2MoO_6 (unmilled) and 5h ball-milled samples.

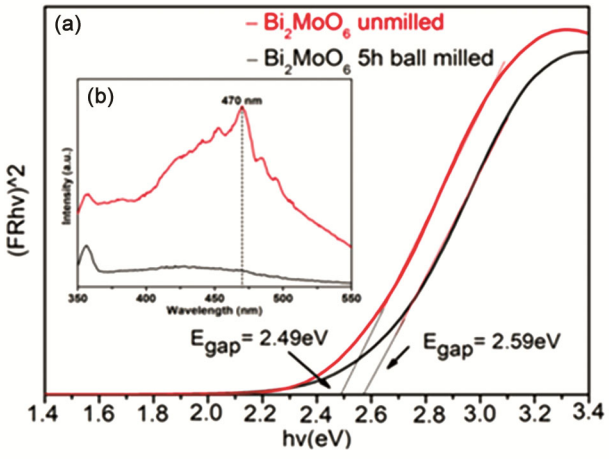

Fig. 3 — The optical band gap of unmilled and 5h ball-milled Bi_2MoO_6. The Inset fig shows the fluorescence spectra.

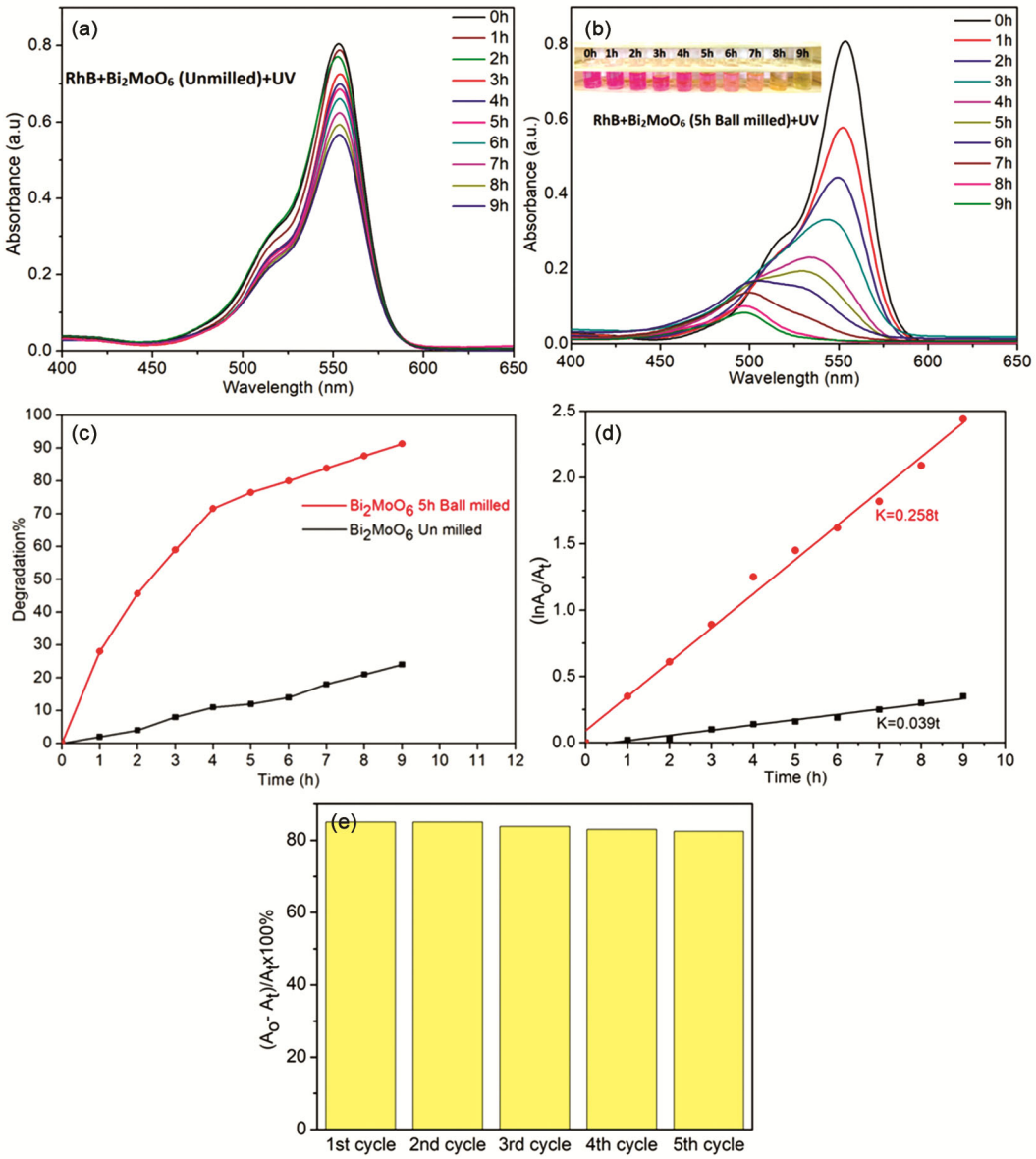

Fig. 4 — shows the photocatalytic activity of; (a) unmilled (b) 5h milled (c) degradation rate and (d) reaction rate constant (e) reusability rate of Bi_2MoO_6 on RhB up to 9h UV irradiation.

already been reported in the literature[39-42]. Figure 4 (c-d) shows the degradation efficiency and the reaction rate constant respectively.

A recycling photocatalytic experiment was conducted to study the stability and reusability efficiency of the prepared photocatalyst. Figure 4(e) depicts that Bi_2MoO_6 particles have excellent reusability properties. The degradation efficiency of the photocatalyst is maintained after 5 cycles**.** The prepared Bi_2MoO_6 photocatalyst after a cyclic run was collected and studied under an x-ray diffractometer. No changes in the XRD pattern of used and fresh photocatalyst are observed, depicting that the Bi_2MoO_6 sample is structurally stable.

4 Discussion

UV light irradiation excited Bi_2MoO_6 which ultimately produced the photogenerated charge carriers. The photogenerated electrons react with oxygen and produce anionic superoxide radical (O_2^-) whereas, the photogenerated holes react with water to form OH* radical. The superoxide radical undergoes the protonation process and produces hydroperoxyl radical (HOO*). The formed OH* is a powerful

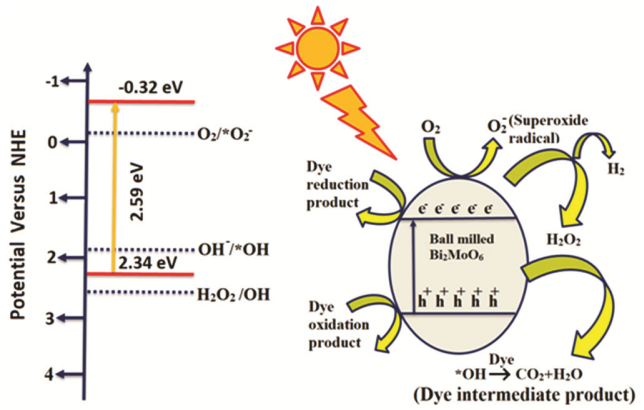

Fig. 5 — Pictorial representation of photocatalytic degradation of dye by Bi_2MoO_6 powder.

oxidizing agent. Thus the surface of the photoexcited photocatalyst undergoes both oxidation and reduction process[43-45]. From the literature we know that IPA is used as a scavenger of OH*, BQ is a scavenger of OH* and $*O^{2-}$ respectively. And AO is an efficient scavenger of h^+. The investigation of primary active species responsible for RhB degradation by Bi_2MoO_6, in the presence of various scavengers, has been performed by Jiang *et al.*[46] showed that the addition of IPA shows no influence on RhB removal whereas, the addition of BQ or AO reduces the photocatalytic degradation of RhB. The above result explains the superiority of h^+ and $*O^{2-}$ in RhB removal and the trivial role of *OH.

The conduction band and the valence band potential play an essential part in the explanation of the photocatalytic activity. For pure Bi_2MoO_6 Mo 4d, Bi 6p and O 2p orbitals present for conduction band, and Bi 6s and O 2p orbitals present for valence band[47-48]. The valence band and conduction band potential has been calculated by Millikan's equation [49] which is represented as

$$E_{CB} = X - E_c - \frac{E_g}{2}$$

$$E_{VB} = E_{CB} - E_g$$

Where, X represents the mean of electron affinity and ionization potential and is reported to be 5.5 eV in the literature[50]. The E_c is the kinetic energy of free electrons of the hydrogen scale which is reported to be 4.5eV, and E_g is the optical band gap of Bi_2MoO_6 (ball-milled) which was calculated to be 2.59eV. The conduction band and valence band potential of ball-milled Bi_2MoO_6 versus normal hydrogen electrode were calculated to be -0.32 and 2.34 eV. This is shown in Fig. 5 along with the pictorial representation of Photo catalytic degradation of RhB. The conduction band potential of Bi_2MoO_6 is more negative than $O_2/*O_2^-$ (+0.13V)[51]. This makes the reaction between O_2 and e^- possible, producing $*O_2^-$, which decomposes RhB pollutants. Meanwhile, the valence band potential of ball-milled Bi_2MoO_6 is negative to the redox potential of $H_2O/*OH$ (+2.68eV)[51]. Thus, the photoexcited h^+ can react with OH^- and H_2O to give *OH radicals. However, the scavenger test proves that there is no *OH evolved.

5 Conclusion

In the present study, Bi_2MoO_6 was successfully synthesized by using the SSR route. The ball milling technique was employed to reduce the size of the grain particles of the prepared sample. The crystallite size got reduced from 96 to 35nm. The photocatalytic activity of unmilled and 5h ball-milled Bi_2MoO_6 was observed in degrading RhB. The 5h ball-milled Bi_2MoO_6 showed remarkable degradation efficiency than unmilled Bi_2MoO_6. Thus there exists a relation between electron surface area and electron mobility which plays an important effect on the catalyst's photocatalytic behaviour.

Acknowledgement

The authors thank the Department of Science and Technology, Govt. of India, for providing financial assistance to the above research work through the WOS-A Fellowship (SR/WOS-A/CS-128/2018).

References

1 Fujishima A & Honda K, *Nature*, 238 (1972) 37.
2 Vidyasagar D, Manwar N, Gupta A, Ghugal S G, Umare S S & Boukherroub R, *Catal Sci Technol*, 9 (2019) 822.
3 Heidarpour H, Padervand M, Soltanieh M & Vossoughi M, *Chem Eng Res Des*, 153 (2020) 709.
4 Elahifard M R, Behjatmanesh-Ardakani R, Ahmadvand S & Abbasi B, *Res Chem Intermed*, 45 (2019) 4885.
5 Padervand M, Lammel G, Bargahi A & Mohammad-Shiri H, *Nano-Struct Nano-Objects*, 18 (2019) 100258.
6 Saleh T A & Gupta V K, *J Colloid Interface Sci*, 371 (2012) 101.
7 Saleh T A & Gupta, V K, *J Colloid Interface Sci*, 362 (2011) 337.
8 Saravanan R, Gupta V K, Narayanan V & Stephen A, *J Taiwan Inst Chem Eng*, 45 (2014) 1910.
9 Saravanan R, Gupta V K, Mosquera E & Gracia F, *J Mol Liq*, 198 (2014) 409.
10 Saravanan R, Sacari E, Gracia F, Khan M M, Mosquera E & Gupta V K, *J Mol Liq*, 221 (2016) 1029.
11 Saravanan R, Khan M M, Gupta V K, Mosquera E, Gracia F, Narayanan V & Stephen A J J O C, *J Mol Liq*, 452 (2015) 126.
12 Saravanan R, Karthikeyan S, Gupta V K, Sekaran G, Narayanan V & Stephen A J M S, *Mater Sci Eng C*, 33 (2013) 91.

13 Zhang L W, Wang Y J, Cheng H Y, Yao W Q & Zhu Y F, *Adv Mater*, 21 (2009) 1286.
14 Xu H, Wang W & Zhu W, *J Phys Chem B*, 110 (2006) 13829.
15 Li G, Huang S, Shen Y, Lou Z, Yuan H, Zhu N & Wei Y, *Dalton Trans*, 48 (2019) 9925.
16 Gnanam S & Rajendran V, *J Alloys Compd*, 735 (2018) 1854.
17 Ranjith K S, Saravanan P, Vinod V T P, Filip J, Černík M & Kumar R R, *Catal Today*, 278 (2016) 271.
18 Lin M, Fu Z Y, Tan H R, Tan J P Y, Ng S C & Teo E, *Cryst Growth Des*, 12 (2012) 3296.
19 Yao H, Wang Y & Luo G, *Ind Eng Chem Res*, 56 (2017) 4993.
20 Shifu C, Mingsong J & Yunguang Y, *J Nanosci*, 12 (2012) 4898.
21 Vatanparast M & Saedi L, *J Mater Sci Mater Electron*, 29 (2018) 7107.
22 Chankhanittha T, Somaudon V, Watcharakitti J, Piyavarakorn V & Nanan S, *Mater Lett*, 258 (2020) 126764.
23 Phuruangrat A, Putdum S, Dumrongrojthanath P, Thongtem S & Thongtem T, *J Nanomater*, 2015.
24 Shetty M, Murthy M, Shastri M, Sindhusree M, Nagaswarupa H P, Shivaramu P D & Rangappa D, *Ceram Int*, 45 (2019) 24965.
25 Zhang L, Xu T, Zhao X & Zhu Y, *Appl Catal B*, 98 (2010) 138.
26 Hejazi R, Mahjoub A R & Khavar A H C, *Solid State Sci*, 95 (2019) 105934.
27 Li H, Liu C, Li K & Wang H, *J Mater Sci*, 43 (2008) 7026.
28 Liang D, Ding Y, Wang N, Cai X, Li J, Han L, Wang S, Han Y, Jia G & Wang L, *Mod Phys Lett B*, *31* (2017) 1750241.
29 Cheng L, Liu L, Wang D, Yang F & Ye J, *J CO2 Util*, 29 (2019) 196.
30 Schuh K, Kleist W, Hoj M, Trouillet V, Beato P, Jensen A D & Grunwaldt J D, *Catal*, 5 (2015) 1554.
31 Murugan R, *Physica B Condens,* 352 (2004) 227.
32 Liu Z, Tian J, Zeng D, Yu C, Huang W, Yang K, Liu X & Liu H, *Mater Res Bul*, 112 (2019*)* 336.
33 Liu X, Wang J, Dong Y, Li H, Xia Y & Wang H, *Mater Sci Semicond Process*, 88 (2018) 214.
34 Sun C, Xu Q, Xie Y, Ling Y, Jiao J, Zhu H, Zhao J, Liu X, Hu B & Zhou D, *J Alloys Comp*, 723 (2017) 333.
35 Maczka M, Paraguassu W, Souza Filho A G, Freire P T C, Mendes Filho J & Hanuza J, *Phys Rev*, 77 (2008) 094137.
36 Zhou Y, Zhang Y, Lin M, Long J, Zhang Z, Lin H, Wu J C S & Wang X, *Nat Commun*, 6 (2015) 1.
37 Loyalka S K & Riggs C A, *J Appl Spectrosc*, 49 (1995) 1107.
38 Fujihara K, Izumi S, Ohno T & Matsumura M, *J Photochem Photobiol*, 132 (2000) 99.
39 Ma Y & Yao J N, *J Photochem Photobiol*, 116 (1998) 167.
40 Watanabe T, Takizawa T & Honda K, *J Phys Chem Lett*, 81 (1977) 1845.
41 Takizawa T, Watanabe T & Honda K, *J Phys Chem Lett*, 82 (1978) 1391.
42 López S M, Hidalgo M C, Navío J A & Colón G, *J Hazard Mater*, 185 (2011) 1425.
43 Tanaka K, Padermpole K & Hisanaga T, *Water Res*, 34 (2000) 327.
44 Gouvea C A, Wypych F, Moraes S G, Duran N, Nagata N & Peralta-Zamora P, *Chemosphere*, 40 (2000) 433.
45 Konstantinou I K & Albanis T A, *Appl Catal B*, 49 (2004) 1.
46 Li S, Hu S, Jiang W, Liu Y, Zhou Y, Liu J & Wang Z, *J Colloid Interface Sci*, 530 (2018) 171.
47 Meng X & Zhang Z, *Appl Catal B*, 209 (2017) 383.
48 Bi J, Wu L, Li J, Li Z, Wang X & Fu X, *Acta Mater,*55 (2007) 4699.
49 Morrison S R, *Electrochemistry at semiconductor and oxidized metal electrodes* (New York: Plenum) 1980.
50 Li S, Shen X, Liu J & Zhang L, *Environ Sci Nano*, 4 (2017) 1155.
51 Chen Y, Tian G, Shi Y, Xiao Y & Fu H, *Appl Catal B*, 164 (2015) 40.